(Preprint) AAS 25-628

A GENERAL GAUSSIAN STEERING FRAMEWORK LEVERAGING NONLINEARITY CONSTRAINTS

William N. Fife*, Jackson Kulik†, and Kyle J. DeMars‡

Gaussian steering has been proposed in the literature as a means of constructing—*a priori*—a feedback law to control the mean and covariance of state dispersions. The primary astrodynamics application is the ability to develop nominal and correction maneuvers for a spacecraft that are robust to modeled uncertainties, such as orbit determination and maneuver execution. An additional goal for Gaussian steering is that robustness to uncertainties is claimed as a result of a successful optimization and not as a product of Monte Carlo verification. To that end, this paper develops a general Gaussian steering framework for nonlinear systems with affine control input where an additional constraint based on the system's nonlinearity is inserted. The generalized aspect comes from the ability to evaluate expectations via analytical linearization or quadrature. The approach is demonstrated in various simulated examples commonly used in the literature.

INTRODUCTION

A principal component of spacecraft maneuver design is ensuring that the statistical dispersions of both the spacecraft state and control usage are minimized or constrained. In practice, this process is separated into a trajectory design step (i.e., optimal control[1]) and an uncertainty quantification step, where the latter informs changes to the former and the process is repeated. Not only is this procedure overly time consuming for potential onboard applications, it also lacks the infrastructure to *assign* statistical constraints within the optimization step itself. The same problem exists in other domains where optimized control sequences must be resilient to uncertainties, such as entry, descent, and landing.[2] Alternatively, covariance control or *Gaussian steering* directly embeds the evolution of uncertainty parameters, namely mean and covariance, into the optimization along with desired statistical constraints.[3] Gaussian steering is a subset of stochastic control approaches that include stochastic dynamic programming and unscented trajectory optimization.[4]

In Gaussian steering, parameters of a feedback control law are optimized while ensuring that the evolution of the state mean and covariance satisfy various criteria. A multitude of implementations have been presented in the literature for linear systems[5–7] and nonlinear systems.[8–10] One standard approach is to develop a representative nonlinear programming (NLP) problem—where the optimization variables are the set of open loop controls and feedback gains—and solve it via off-the-shelf NLP solvers. Another common approach is to make all parts of the NLP problem convex by linearizing the dynamics about a nominal trajectory and/or an initial guess of the optimization variables, then iteratively solving convex programs (i.e., successive convexification). These two approaches stem from the same originating NLP but can result in distinct optimal values. In this work, a general architecture is presented where the driving source of non-convexity—the nonlinear

*PhD Candidate, Department of Aerospace Engineering, Texas A&M University, College Station, TX.
†Assistant Professor, Mechanical and Aerospace Engineering, Utah State University, Logan, UT.
‡Associate Professor, Department of Aerospace Engineering, Texas A&M University, College Station, TX.

dynamics—can be dealt with either by analytical linearization or statistical linearization (i.e., Gaussian quadrature). Quadrature eliminates the analytical linearization of the dynamics and statistical constraints but with an increase in computational expense. In the case of analytical linearization, the successive convexification technique can be recovered without further approximations using lossless relaxations previously discovered.[7]

A natural benefit of Gaussian steering for linear systems is that—despite modeled uncertainties—theoretical guarantees of constraint satisfaction is a product of a successful optimization. This feature is akin to that of the Kalman filter exactly characterizing the covariance of the true estimation error distribution and is termed *covariance realism*. The guarantee of covariance realism vanishes in the presence of nonlinear dynamics due to the required approximations. To that end, this work develops an additional constraint based on the system's underlying nonlinearity as measured by a semianalytical measure.[11,12] The result is a more constrained optimization problem that bounds the state dispersions within a region of the state space where linear approximations are well-suited.

This work is organized as follows. First, the general Gaussian steering framework is outlined along with the traditional assumptions made. Two implementations—analytical linearization and quadrature—are developed along with a description of a special lossless convexification case. Then, the measure of nonlinearity constraint, and how it is embedded into the optimization, is discussed. Finally, the approach is applied to a Near Rectilinear Halo Orbit (NRHO) maneuver planning scenario and tested in Monte Carlo simulations.

GAUSSIAN STEERING FOR NONLINEAR-AFFINE SYSTEMS

Consider a stochastic state $\boldsymbol{x} \in \mathbb{R}^n$ governed by discrete, nonlinear-affine dynamics of the form

$$\boldsymbol{x}_k = \boldsymbol{f}(\boldsymbol{x}_{k-1}) + \boldsymbol{F}_u \boldsymbol{u}_{k-1}(\boldsymbol{x}_{k-1}) + \boldsymbol{w}_{k-1}\,, \tag{1}$$

where $\boldsymbol{w} \in \mathbb{R}^p$ is a zero-mean, Gaussian process noise term with known covariance $\boldsymbol{P}_{ww}$. The process noise is assumed to be uncorrelated with the state at all times, and is used to model both epistemic and aleatoric uncertainties. The control $\boldsymbol{u} \in \mathbb{R}^m$ is applied at discrete nodes via the control mapping matrix $\boldsymbol{F}_u$ and, importantly, $\boldsymbol{u}$ is a function of the state $\boldsymbol{x}_{k-1}$. Equation (1) is a common preliminary model for astrodynamics scenarios employing impulsive control. Continuous forms of $\boldsymbol{f}(\cdot)$ in Equation (1) can also be considered by assuming $\boldsymbol{f}(\cdot)$ is the result of numerical integration. At the initial time t_0, the set of all possible states is characterized by a given Gaussian probability density function (pdf) $p(\boldsymbol{x}_0) = p_g(\boldsymbol{x}_0; \boldsymbol{m}_{x,0}, \boldsymbol{P}_{xx,0})$, where $p_g((\cdot); \boldsymbol{m}_{(\cdot)}, \boldsymbol{P}_{(\cdot)})$ is a multivariate Gaussian pdf with mean $\boldsymbol{m}_{(\cdot)}$ and covariance $\boldsymbol{P}_{(\cdot)}$. The objective is to compute a set of feedback controls $\bar{\boldsymbol{u}} = \{\boldsymbol{u}_0, \boldsymbol{u}_1, ..., \boldsymbol{u}_{N-1}\}$ that steer the state pdf from $p(\boldsymbol{x}_0)$ to some prescribed Gaussian pdf $p_g(\boldsymbol{x}_f; \boldsymbol{m}_{x,f}, \boldsymbol{P}_{xx,f})$ in a given finite interval $t \in [t_0, t_N]$ by minimizing a scalar performance index J and while adhering to potential path constraints on the control and state.

It is important to acknowledge here that $p(\boldsymbol{x}_0)$ represents the *true* dispersions and not an observer's estimate of them. In the subsequent developments, the assumption is that the feedback controls $\bar{\boldsymbol{u}}$ are enacted with zero estimation uncertainty (i.e., full state feedback). For linear-Gaussian systems, observer estimation error can be incorporated without approximation using the separation theorem[1]. Approximations are required for nonlinear systems, with the prevalent approach being linearization of the observer uncertainty propagation equations along a reference trajectory[13,14]. This effectively results in an additional source of uncertainty that further constrains the *true* dispersions compared to the case with perfect observer knowledge.

In this work, the boundary constraints on the state are the aforementioned pdf prescriptions, and the path constraints are given by the dynamics in Equation (1). The control has path constraints

given by the expectation,

$$\| \mathbb{E}\{\boldsymbol{u}_k\}\| + \gamma \|\mathcal{S}\{\boldsymbol{u}_k\}\|_F \leq \rho_u \qquad \forall\, k \in [0, N-1]\,, \tag{2}$$

where ρ_u is the control magnitude bound, γ is a scaling parameter, $\|\cdot\|_F$ is the Frobenius norm, $\mathbb{E}\{\cdot\}$ is the expectation operator, and $\mathcal{S}\{\cdot\}$ is the covariance operator defined by $\mathcal{S}\{\boldsymbol{a}\} = \mathbb{E}\{[\boldsymbol{a} - \mathbb{E}\{\boldsymbol{a}\}][\boldsymbol{a} - \mathbb{E}\{\boldsymbol{a}\}]^T\}$. While most of the Gaussian steering literature applies the chance-constraint $P(\|\boldsymbol{u}_k\| \leq \rho_u) \geq 1-\epsilon$ for bounding the control magnitude (see References 8–10 and 14) this work chooses Equation (2) based on the following arguments. Firstly, the deterministic analogs developed in the aforementioned references for the chance constraint are themselves relaxations, and different formulations result in more or less conservatism (see Table 1 in Reference 14). Secondly, as will be discussed, the nonlinearities in the problem result in a lack of guarantee of Gaussianity, and, therefore, selection of the allowable probability violation (i.e., the value of ϵ) is arbitrary until statistically proven.

The performance index is typically prescribed as expectations of a nonlinear function of the states and controls; that is,

$$J = \mathbb{E}\{g(\bar{\boldsymbol{u}}, \bar{\boldsymbol{x}})\} + c \cdot \mathcal{S}\left\{g(\bar{\boldsymbol{u}}, \bar{\boldsymbol{x}})\right\}\,, \tag{3}$$

where $g(\cdot)$ is a deterministic nonlinear function of the concatenation of all control and state parameters $\bar{\boldsymbol{u}}$ and $\bar{\boldsymbol{x}}$, respectively, and c is a scaling parameter to align the units of J and weight the covariance index relative to the mean index. It is not required that both $\mathbb{E}\{\cdot\}$ and $\mathcal{S}\{\cdot\}$ be present in the objective. The problem, as developed thus far, is expressed as

$$\min_{\bar{\boldsymbol{u}}, \bar{\boldsymbol{x}}} \quad \mathbb{E}\{g(\bar{\boldsymbol{u}}, \bar{\boldsymbol{x}})\} + c \cdot \mathcal{S}\left\{g(\bar{\boldsymbol{u}}, \bar{\boldsymbol{x}})\right\}\,, \tag{4a}$$

subject to path constraints

$$\boldsymbol{x}_k = \boldsymbol{f}(\boldsymbol{x}_{k-1}) + \boldsymbol{F}_u \boldsymbol{u}_{k-1}(\boldsymbol{x}_{k-1}) + \boldsymbol{w}_{k-1} \qquad \forall k \in [0, N-1] \tag{4b}$$

$$\| \mathbb{E}\{\boldsymbol{u}_k\}\| + \gamma \|\mathcal{S}\{\boldsymbol{u}_k\}\|_F \leq \rho_u \qquad \forall k \in [0, N-1] \tag{4c}$$

and terminal constraint

$$\boldsymbol{x}_N \sim p_g(\boldsymbol{x}_f; \boldsymbol{m}_{x,f}, \boldsymbol{P}_{xx,f})\,. \tag{4d}$$

Equations (4) represent a generic optimization for the nonlinear-affine, Gaussian steering problem. Note that since $\boldsymbol{u}_{k-1}$ in Equation (4b) is itself a function and due to Equation (4c), this problem as posed is infinite dimensional. The problem is made finite by parameterizing the control via

$$\boldsymbol{u}_{k-1}(\boldsymbol{x}_{k-1}) = \boldsymbol{v}_{k-1} + \boldsymbol{G}_{k-1}[\boldsymbol{x}_{k-1} - \boldsymbol{m}_{x,k-1}]\,, \tag{5}$$

where $\boldsymbol{v}_{k-1}$ represents a nominal or open loop control and $\boldsymbol{G}_{k-1}$ is a feedback gain matrix operating on the discrepancy between the true state and the expected (mean) state $\boldsymbol{m}_{x,k-1}$ at time t_{k-1}. Both $\boldsymbol{v}_{k-1}$ and $\boldsymbol{G}_{k-1}$ are deterministic. Computing the mean and covariance of Equation (5) gives

$$\begin{aligned} \mathbb{E}\{\boldsymbol{u}_{k-1}\} &= \boldsymbol{v}_{k-1} \\ \mathcal{S}\{\boldsymbol{u}_{k-1}\} &= \boldsymbol{G}_{k-1} \boldsymbol{P}_{xx,k-1} \boldsymbol{G}_{k-1}^T\,, \end{aligned}$$

where $\boldsymbol{P}_{xx,k-1}$ is the state covariance at t_{k-1}. Additionally, Equation (4d) is relaxed into separate mean and covariance constraints

$$\mathbb{E}\{\boldsymbol{x}_N\} \triangleq \boldsymbol{m}_{x,N} = \boldsymbol{m}_{x,f} \tag{7a}$$

$$\mathcal{S}\{\boldsymbol{x}_N\} \triangleq \boldsymbol{P}_{xx,N} \preceq \boldsymbol{P}_{xx,f}\,, \tag{7b}$$

as is typically done in the literature[3,5]. Note that $\boldsymbol{A} \preceq \boldsymbol{B}$ is used to denote that the difference $\boldsymbol{B} - \boldsymbol{A} \succeq \boldsymbol{0}$ (i.e., the difference is positive semidefinite). The constraint in Equation (7b) can be implemented in a variety of ways, depending on the nature of the optimization problem. With these modifications, the optimization variables become the concatenated set of open loop controls $\bar{\boldsymbol{v}}$, feedback matrices $\bar{\boldsymbol{G}}$, and state means $\bar{\boldsymbol{m}}_x$ and covariances $\bar{\boldsymbol{P}}_{xx}$. Letting $\boldsymbol{\theta} = \{\bar{\boldsymbol{v}}, \bar{\boldsymbol{G}}, \bar{\boldsymbol{m}}_x, \bar{\boldsymbol{P}}_{xx}\}$, the problem is thus expressed as

$$\min_{\boldsymbol{\theta}} \quad \mathbb{E}\{g(\boldsymbol{\theta})\} + c \cdot \mathcal{S}\left\{g(\boldsymbol{\theta})\right\}\,, \tag{8a}$$

subject to path constraints

$$\boldsymbol{x}_k = \boldsymbol{f}(\boldsymbol{x}_{k-1}) + \boldsymbol{F}_u(\boldsymbol{v}_{k-1} + \boldsymbol{G}_{k-1}[\boldsymbol{x}_{k-1} - \boldsymbol{m}_{x,k-1}]) + \boldsymbol{w}_{k-1} \qquad \forall k \in [1, N] \tag{8b}$$

$$\|\boldsymbol{v}_k\| + \gamma\|\boldsymbol{G}_k\boldsymbol{P}_{xx,k}\boldsymbol{G}_k^T\|_F \leq \rho_u \qquad \forall k \in [0, N-1] \tag{8c}$$

and terminal constraints

$$\boldsymbol{m}_{x,N} = \boldsymbol{m}_{x,f} \tag{8d}$$

$$\boldsymbol{P}_{xx,N} \preceq \boldsymbol{P}_{xx,f}\,. \tag{8e}$$

It should be noted that the given problem data for Equations (8) are $\boldsymbol{m}_{x,0}$, $\boldsymbol{P}_{xx,0}$, $\boldsymbol{m}_{x,f}$, $\boldsymbol{P}_{xx,f}$, $\boldsymbol{F}_u$, ρ_u, and P_u. For a given function $g(\boldsymbol{\theta})$, Equations (8) describe a nonlinear program. However, it is still undefined how the state means $\boldsymbol{m}_x$ and covariances $\boldsymbol{P}_{xx}$ are related through the dynamics. What follows are two approaches to implement Equations (8) that differ in how the nonlinear function $\boldsymbol{f}(\cdot)$ is handled.

Linearized Formulation

Assume a reference trajectory is generated, for all $k \in [1, N]$, by $\hat{\boldsymbol{x}}_k = \boldsymbol{f}(\hat{\boldsymbol{x}}_{k-1})$, where $\hat{\boldsymbol{x}}_0 = \boldsymbol{m}_{x,0}$. The right-hand side of Equation (8b) can be linearized about $\hat{\boldsymbol{x}}$ such that

$$\boldsymbol{x}_k = \boldsymbol{F}_x(\hat{\boldsymbol{x}}_{k-1})\boldsymbol{x}_{k-1} + \boldsymbol{F}_u\boldsymbol{G}_{k-1}[\boldsymbol{x}_{k-1} - \boldsymbol{m}_{x,k-1}] + \boldsymbol{c}_{k-1} + \boldsymbol{w}_{k-1}\,, \tag{9}$$

where $\boldsymbol{c}_{k-1} = \boldsymbol{f}(\hat{\boldsymbol{x}}_{k-1}) - \boldsymbol{F}_x(\hat{\boldsymbol{x}}_{k-1})\hat{\boldsymbol{x}}_{k-1} + \boldsymbol{F}_u\boldsymbol{v}_{k-1}$ and $\boldsymbol{F}_x$ is the Jacobian $\partial\boldsymbol{f}/\partial\boldsymbol{x}$. Letting $\hat{\boldsymbol{F}}_{x,k-1} = \boldsymbol{F}_x(\hat{\boldsymbol{x}}_{k-1})$ and assuming $\boldsymbol{F}_x$ is a deterministic quantity, the expectation of Equation (9) gives the linearized mean dynamics as

$$\boldsymbol{m}_{x,k} = \hat{\boldsymbol{F}}_{x,k-1}\boldsymbol{m}_{x,k-1} + \boldsymbol{c}_{k-1}\,, \tag{10}$$

and computing the covariance of Equation (9) gives

$$\boldsymbol{P}_{xx,k} = [\hat{\boldsymbol{F}}_{x,k-1} + \boldsymbol{F}_u\boldsymbol{G}_{k-1}]\boldsymbol{P}_{xx,k-1}[\hat{\boldsymbol{F}}_{x,k-1} + \boldsymbol{F}_u\boldsymbol{G}_{k-1}]^T + \boldsymbol{P}_{ww}\,. \tag{11}$$

Equation (8b) is then replaced with Equations (10) and (11). Since Equations (10) and (11) are themselves dependent on the open loop controls $\bar{\boldsymbol{v}}$ and feedback gains $\bar{\boldsymbol{G}}$, the optimization variables set is reduced to $\boldsymbol{\theta} = \{\bar{\boldsymbol{v}}, \bar{\boldsymbol{G}}\}$ and the problem is expressed as

$$\min_{\boldsymbol{\theta}} \quad \mathbb{E}\{g(\boldsymbol{\theta})\} + c \cdot \mathcal{S}\left\{g(\boldsymbol{\theta})\right\}\,, \tag{12a}$$

subject to path constraints

$$\boldsymbol{m}_{x,k} = \hat{\boldsymbol{F}}_{x,k-1}\boldsymbol{m}_{x,k-1} + \boldsymbol{f}(\hat{\boldsymbol{x}}_{k-1}) - \hat{\boldsymbol{F}}_{x,k-1}\hat{\boldsymbol{x}}_{k-1} + \boldsymbol{F}_u\boldsymbol{v}_{k-1} \qquad \forall k \in [1, N] \tag{12b}$$

$$\boldsymbol{P}_{xx,k} = [\hat{\boldsymbol{F}}_{x,k-1} + \boldsymbol{F}_u\boldsymbol{G}_{k-1}]\boldsymbol{P}_{xx,k-1}[\hat{\boldsymbol{F}}_{x,k-1} + \boldsymbol{F}_u\boldsymbol{G}_{k-1}]^T + \boldsymbol{P}_{ww,k-1} \qquad \forall k \in [1,N] \quad (12c)$$

$$\|\boldsymbol{v}_k\| + \gamma\|\boldsymbol{G}_k\boldsymbol{P}_{xx,k}\boldsymbol{G}_k^T\|_F \leq \rho_u \qquad \forall k \in [0,N-1] \quad (12d)$$

and terminal constraints

$$\boldsymbol{m}_{x,N} = \boldsymbol{m}_{x,f} \quad (12e)$$

$$\boldsymbol{P}_{xx,N} \preceq \boldsymbol{P}_{xx,f}\,. \quad (12f)$$

Equations (12) is a linearized Gaussian steering problem assuming a form for the feedback control given by Equation (5). Alongside the previously defined problem data, the reference trajectory $\hat{\boldsymbol{x}}_k\ \forall k$ is supplied as an input to the optimization problem. For the variable set $\boldsymbol{\theta} = \{\bar{\boldsymbol{v}}, \bar{\boldsymbol{G}}\}$, this problem is nonconvex and can be solved via many nonlinear programming techniques.[15] However, as References 7, 13, and 16 show, an expansion of the optimization variables for a specific kind of performance index $g(\boldsymbol{\theta})$ results in a convex program.

Special Case of Convex Optimization For the function,

$$g = \sum_{k=0}^{N-1}[\boldsymbol{x}_k - \boldsymbol{m}_{x,k}]^T\boldsymbol{G}_k^T\boldsymbol{G}_k[\boldsymbol{x}_k - \boldsymbol{m}_{x,k}] + \boldsymbol{v}_k^T\boldsymbol{v}_k\,,$$

and discarding the variance of g, the performance index becomes

$$J = \sum_{k=0}^{N-1}\text{tr}\{\boldsymbol{G}_k\boldsymbol{P}_{xx,k}\boldsymbol{G}_k^T\} + \boldsymbol{v}_k^T\boldsymbol{v}_k\,.$$

Creating two new sets of optimization variables

$$\boldsymbol{U}_k \triangleq \boldsymbol{G}_k\boldsymbol{P}_{xx,k}$$
$$\boldsymbol{Y}_k \triangleq \boldsymbol{G}_k\boldsymbol{P}_{xx,k}\boldsymbol{G}_k^T\,,$$

a new optimization problem can be posed as

$$\min_{\boldsymbol{m}_{x,k},\boldsymbol{v}_k,\boldsymbol{P}_{xx,k},\boldsymbol{U}_k,\boldsymbol{Y}_k} \quad \sum_{k=0}^{N-1}\text{tr}\{\boldsymbol{Y}_k\} + \boldsymbol{v}_k^T\boldsymbol{v}_k\,, \quad (13a)$$

subject to path constraints

$$\boldsymbol{m}_{x,k} = \hat{\boldsymbol{F}}_{x,k-1}\boldsymbol{m}_{x,k-1} + \boldsymbol{f}(\hat{\boldsymbol{x}}_{k-1}) - \hat{\boldsymbol{F}}_{x,k-1}\hat{\boldsymbol{x}}_{k-1} + \boldsymbol{F}_u\boldsymbol{v}_{k-1} \qquad \forall k \in [1,N] \quad (13b)$$

$$\begin{aligned}\boldsymbol{P}_{xx,k} = {} & \hat{\boldsymbol{F}}_{x,k-1}\boldsymbol{P}_{xx,k-1}\hat{\boldsymbol{F}}_{x,k-1}^T + \boldsymbol{F}_u\boldsymbol{U}_{k-1}\hat{\boldsymbol{F}}_{x,k-1}^T \\ & + \hat{\boldsymbol{F}}_{x,k-1}\boldsymbol{U}_{k-1}^T\boldsymbol{F}_u^T + \boldsymbol{F}_u\boldsymbol{Y}_{k-1}\boldsymbol{F}_u^T + \boldsymbol{P}_{ww,k-1} \qquad \forall k \in [1,N]\end{aligned} \quad (13c)$$

$$\|\boldsymbol{v}_k\| + \gamma\|\boldsymbol{Y}_k\|_F \leq \rho_u \qquad \forall k \in [0,N-1] \quad (13d)$$

$$\begin{bmatrix}\boldsymbol{P}_{xx,k} & \boldsymbol{U}_k^T \\ \boldsymbol{U}_k & \boldsymbol{Y}_k\end{bmatrix} \succeq \boldsymbol{0} \qquad \forall k \in [0,N-1] \quad (13e)$$

and terminal constraints

$$\boldsymbol{m}_{x,N} = \boldsymbol{m}_{x,f} \quad (13f)$$

$$\boldsymbol{P}_{xx,N} \preceq \boldsymbol{P}_{xx,f}\,. \quad (13g)$$

Equations (13) form a convex program since the performance index and constraints are all convex functions of the optimization variables. The relaxation stems from the linear matrix inequality

of Equation (13e) allowing for $\boldsymbol{Y}_{k-1} \neq \boldsymbol{G}_{k-1}\boldsymbol{P}_{xx,k-1}\boldsymbol{G}_{k-1}^T$. However, it has been shown that, at optimality, it is indeed the case that $\boldsymbol{Y}_{k-1} = \boldsymbol{G}_{k-1}\boldsymbol{P}_{xx,k-1}\boldsymbol{G}_{k-1}^T$, and, thus, the relaxation is *lossless*.[16] Though the lossless proof is given in Reference 16 (Section IV), the problem herein also includes Equation (13d) and thus a proof for the case that includes this constraint is given in the Appendix. Although Equations (13) form a convex program, it is still implicitly tied to the *a priori* reference trajectory $\hat{\boldsymbol{x}}$. Accordingly, it is common to employ an iterative approach where the optimal mean trajectory $\boldsymbol{m}_{x,k}\ \forall\ k$ from the previous convex iterate becomes the reference trajectory for the next, i.e., $\hat{\boldsymbol{x}}_k \leftarrow \boldsymbol{m}_{x,k}\ \forall\ k$ until a convergence criteria is met or a maximum iteration limit is exceeded. This approach, along with additional techniques, are detailed thoroughly in References 13, 17 and 18.

Quadrature Formulation

As an alternative to analytical linearization of $\boldsymbol{f}(\cdot)$, consider a set of of N_q weights and points of the form $\{w_m^{(j)}, w_c^{(j)}, \boldsymbol{\mathcal{X}}_{k-1}^{(j)}\}_{j=1}^{N_q}$ that comprise a quadrature rule for expectations with respect to $p_g(\boldsymbol{x}_{k-1}; \boldsymbol{m}_{x,k-1}, \boldsymbol{P}_{xx,k-1})$; that is,

$$\boldsymbol{m}_{x,k-1} = \sum_{j=1}^{N_q} w_m^{(j)} \boldsymbol{\mathcal{X}}_{k-1}^{(j)} \tag{14a}$$

$$\boldsymbol{P}_{xx,k-1} = \sum_{j=1}^{N_q} w_c^{(j)} (\boldsymbol{\mathcal{X}}_{k-1}^{(j)} - \boldsymbol{m}_{x,k-1})(\boldsymbol{\mathcal{X}}_{k-1}^{(j)} - \boldsymbol{m}_{x,k-1})^T . \tag{14b}$$

Common quadrature methods include Gauss-Hermite quadrature[19] and the unscented transform[20]. Note that the weights do not depend on time and thus are constant at every node t_k. Starting from an initial set of points $\boldsymbol{\mathcal{X}}_0^{(j)}, j \in \{1, \ldots, N_q\}$, every point is passed through Equation (8b) via the assignment $\boldsymbol{x}_{k-1} \leftarrow \boldsymbol{\mathcal{X}}_{k-1}^{(j)}$ such that

$$\boldsymbol{\mathcal{X}}_k^{(j)} = \boldsymbol{f}(\boldsymbol{\mathcal{X}}_{k-1}^{(j)}) + \boldsymbol{F}_u(\boldsymbol{v}_{k-1} + \boldsymbol{G}_{k-1}[\boldsymbol{\mathcal{X}}_{k-1}^{(j)} - \boldsymbol{m}_{x,k-1}]) \qquad \forall k \in [1, N] , \tag{15}$$

with the propagated mean $\boldsymbol{m}_{x,k}$ computed using Equation (14a) and propagated covariance given by

$$\boldsymbol{P}_{xx,k} = \boldsymbol{P}_{ww,k-1} + \sum_{j=1}^{N_q} w_c^{(j)} (\boldsymbol{\mathcal{X}}_k^{(j)} - \boldsymbol{m}_{x,k})(\boldsymbol{\mathcal{X}}_k^{(j)} - \boldsymbol{m}_{x,k})^T . \tag{16}$$

Equations (14)-(16) are then leveraged to evaluate Equations (8c)-(8e) within the optimization procedure. Note that the quadrature points themselves need not be optimization variables. The optimization variables can be decreased to $\boldsymbol{\theta} = \{\bar{\boldsymbol{v}}, \bar{\boldsymbol{G}}\}$, just as in the linearization formulation. The benefit of using the quadrature approach is the direct usage of the nonlinear dynamics. The cost is an increased computational burden within the optimization due to the generation of new quadrature points at every node; though, in the absence of process noise, the same quadrature points can be propagated through each node. It is also the case that matrix square-root factors are typically used to compute quadrature points—necessitating additional care in ensuring that the covariance matrices remain positive definite in the optimization process. Further, to the authors' knowledge, there does not exist a special case of lossless convexification of the quadrature formulation due to the presence of $\boldsymbol{f}(\cdot)$ in Equation (15).

COMPARING LINEARIZATION, QUADRATURE, AND CONVEXIFICATION

For comparison, three optimizations of a simple two-dimensional scenario are performed where two implementations use linearization and the third optimization uses quadrature. One of the linearized implementations uses the lossless convexification (denoted as SCVX) from Equations (13).

Let the position $\boldsymbol{r} \in \mathbb{R}^2$ and velocity $\boldsymbol{q} \in \mathbb{R}^2$ of the system evolve according to

$$\begin{aligned} \boldsymbol{r}_k &= \boldsymbol{r}_{k-1} + \Delta t_k \boldsymbol{q}_{k-1} \\ \boldsymbol{q}_k &= (1 - c\|\boldsymbol{q}_{k-1}\|)\boldsymbol{q}_{k-1} + \Delta t_k \boldsymbol{u}_{k-1} + \boldsymbol{w}_{k-1}\,, \end{aligned}$$

where $c > 0$ tunes the nonlinear term in the velocity dynamics and $\boldsymbol{w}$ is the zero-mean, Gaussian process noise. The parameters for this example are given in Table 1 with the units considered to be generic units that are consistent. All three optimizations use the same performance index and problem data. The performance index is taken to be

$$J = \sum_{k=0}^{N-1} \text{tr}\{\boldsymbol{G}_k \boldsymbol{P}_{xx,k} \boldsymbol{G}_k^T\} + \boldsymbol{v}_k^T \boldsymbol{v}_k\,.$$

The nonconvex implementations are solved via the sequential quadratic programming solver SNOPT[21],

Table 1. Optimization parameters for the 2D scenario.

Quantity	Value	Description
c	0.01	Nonlinearity scaling
$\boldsymbol{m}_0$	$[1, 8, 2, 0]^T$	Initial mean
$\boldsymbol{m}_f$	$[1, 2, -1, 0]$	Final mean
$\boldsymbol{P}_{xx,0}$	$0.01 \times \boldsymbol{I}_4$	Initial covariance
$\boldsymbol{P}_{xx,f}$	$0.1 \times \boldsymbol{I}_4$	Final covariance
$\boldsymbol{P}_{ww}$	$10^{-4} \times \boldsymbol{I}_4$	Process noise covariance
Δt	0.6	Time Step
N	25	Nodes
ρ_u	0.3	Mean control constraint
P_u	10^{-3}	Control dispersion constraint

while the lossless convexification is implemented with CVX.[22] The discrete system is propagated with (N, Δt) given in Table 1 with an initial reference control $\hat{\boldsymbol{u}} = [-0.3, 0.1]^T$ used at all nodes $k \in [0, N-1]$. The result is a reference trajectory $\hat{\boldsymbol{x}}$ that is used in the linearized implementations (including SCVX). The initial guess for the nonconvex implementations is given by $\boldsymbol{v}_k = \hat{\boldsymbol{u}}$ and $\boldsymbol{G}_k = \boldsymbol{0}_{m \times n}\ \forall\ k$, while SCVX does not require a user-generated initial guess. For the quadrature implementation, the unscented transform is used to compute quadrature points with parameters $\alpha = 0.1$, $\beta = 2$, and $\kappa = 1$ defined in Reference 20. Lastly, SCVX is iterated over a maximum of 10 iterations or until the norm between successive reference trajectories is less than $\varepsilon = 10^{-3}$.

The optimized position statistics for the linearized, quadrature, and SCVX implementations are shown in Figures 1-3. The illustrated covariance ellipses represent the 99.75% confidence interval. All three implementations satisfy all boundary and path constraints. Although Figures 1-3 are visually similar, a notable difference is that the nonconvex linearization implementation uses heavier feedback control, as seen via the smaller position covariances and velocity uncertainty profile in Fig-

ure 5, where RSS $= \sqrt{\sigma_x^2 + \sigma_y^2}$. This highlights the inverse relationship between state uncertainty $\boldsymbol{P}_{xx}$ and feedback control. Similarly, Figures 4 and 5 show that the SCVX and quadrature implementations use larger amounts of nominal control and less feedback, as seen by the higher velocity uncertainty in Figure 5. This demonstration illustrates the possibility to obtain significantly different results depending on (i) the fundamental problem formulation (i.e., convex vs nonconvex) and (ii) the approach for computing the state mean and covariance within the nonconvex optimizations.

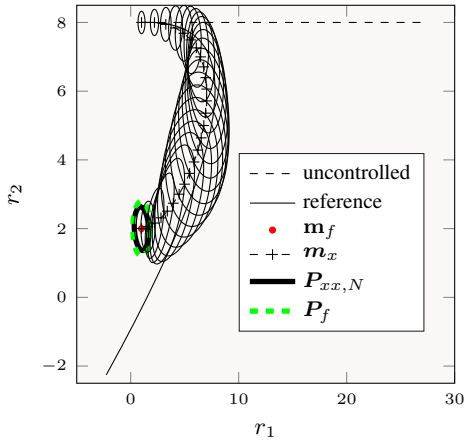

Figure 1. Linearized optimization result.

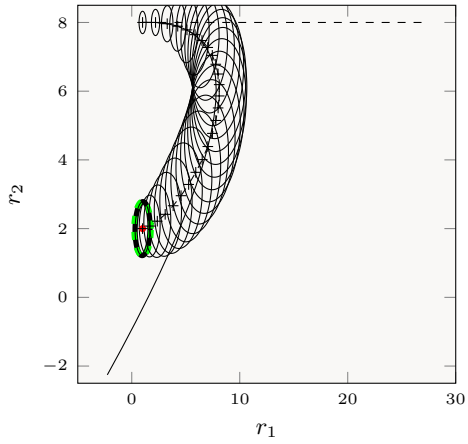

Figure 2. Quadrature optimization result.

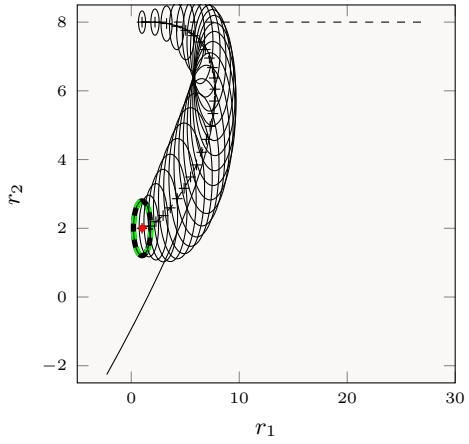

Figure 3. SCVX optimization result.

NONLINEARITY CONSTRAINT VIA TENSOR MEASURE OF NONLINEARITY

The linearization—either analytical or statistical (i.e., quadrature)—invites two interdependent sources of inexactness: truncation and non-Gaussianity. Assuming that the initial state distribution remains Gaussian may degrade the statistical consistency of the method. There are, however, certain locations of the state space where the first-order truncation of the dynamics is a worse approximation than at other locations (i.e., where higher-order terms dominate the linear term). If the state distribution has a large amount of probability mass outside of the region where the linear approximation is valid, then the Gaussian uncertainty model can quickly lose its realism.

To guard against the loss of realism of the Gaussian model, a degree of nonlinearity measure is

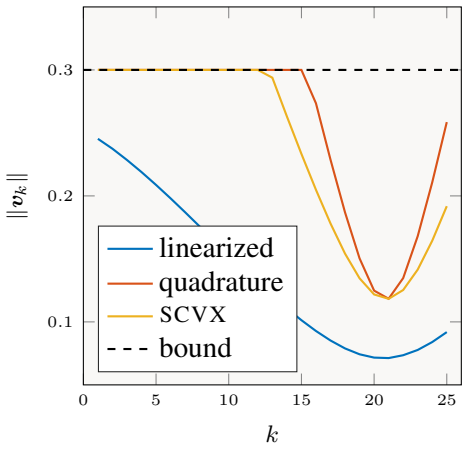

Figure 4. Optimized control magnitude.

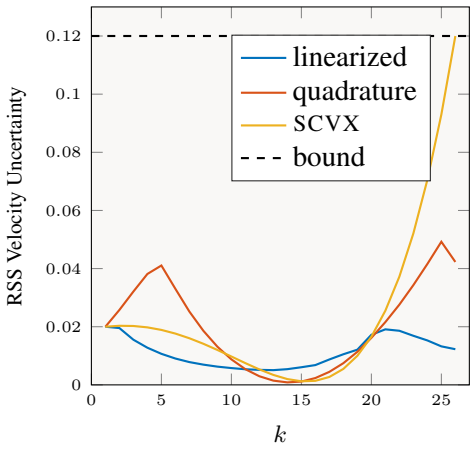

Figure 5. Optimized velocity uncertainty.

embedded as a constraint in the optimization. Various nonlinearity measures have been proposed in the literature with detailed overviews given by Jenson and Scheeres[11] and Kulik.[12] The measure used in this work leverages the induced 2-norm of the second-order state transition tensor.[12] A brief overview of the measure is given here. The measure τ maximizes the 2-norm contribution of the second-order term in the Taylor series expansion of $\boldsymbol{f}(\cdot)$; that is,

$$\tau = \frac{1}{2} \max_{\|\delta \boldsymbol{x}\|=1} \|\boldsymbol{E}_i(\hat{\boldsymbol{F}}_x^{(2)} \delta \boldsymbol{x}^{(2)})\| \,, \tag{17}$$

where $\hat{\boldsymbol{F}}_x^{(i)}$ is the $(i+1)^{\text{th}}$ order tensor related to the i^{th} derivative of $\boldsymbol{f}(\cdot)$, $\delta \boldsymbol{x} = \boldsymbol{x} - \hat{\boldsymbol{x}}$, and $\hat{\boldsymbol{F}}_x^{(i)} \delta \boldsymbol{x}^{(i)}$ describes the i^{th} tensor contraction with $\delta \boldsymbol{x}$, which produces a vector with the same dimensions as $\delta \boldsymbol{x}$. The projection matrix $\boldsymbol{E}_i$ slices the tensor contraction to yield the error for only the i^{th} state. For instance, the position slice for a state vector $\boldsymbol{x} = [\boldsymbol{r}^T \,, \boldsymbol{v}^T]^T$, where $\boldsymbol{r}$ is the position, is $\boldsymbol{E}_r = [\boldsymbol{I} \,, \boldsymbol{0}]$. The maximizations are over the unit ball of dimension identical to $\delta \boldsymbol{x}$. For "small" radii $\delta \boldsymbol{x}$, the second-order contribution should approximate the overall linearization error. The maximizations can be rescaled for a ball of radius α by

$$\tau_\alpha = \alpha^2 \tau \,. \tag{18}$$

The radius α is related to a measure of the size of the state covariance, such as

$$\alpha = \sqrt{\varphi(p, n) \lambda_{\max}(\boldsymbol{P}_{xx})} \,, \tag{19}$$

where $\lambda_{\max}(\cdot)$ is the largest eigenvalue of $\boldsymbol{P}_{xx}$, which is a convex function of $\boldsymbol{P}_{xx}$, and $\varphi(p, n)$ is the inverse cumulative distribution function for a chi-squared distribution with n degrees of freedom and probability gate p. The maximization in Equation (17) has a semianalytical solution requiring a tensor eigenpair computation. From Equations (18) and (19), the constraint at time t_k

$$\varphi(p, n) \lambda_{\max}(\boldsymbol{P}_{xx,k}) \cdot \tau_k \leq \beta_k \tag{20}$$

enforces that the state covariance stays under a size when scaled by the measure of nonlinearity τ_k at the current linearization point $\hat{\boldsymbol{x}}_k$. Note that the form of τ_k is given in Reference 12 and omitted here for brevity, but it suffices to declare τ_k as input data for the optimization. Because τ_k depends on the specific reference trajectory $\hat{\boldsymbol{x}}$, a new τ_k should ideally be computed for every iterate of the

optimization. In practice, the constraint is split into a constraint for each dimension with different units. Thus, the user-defined parameter β_k has identical units to the slice of $\sqrt{\boldsymbol{P}_{xx,k}}$ which has consistent units (e.g., the position-only slice). Equation (20) is an opposing constraint to Equation (2) since, in order to lower the state covariance to satisfy Equation (20), a corresponding increase in feedback control is typically required. Note that, for the lossless convexification of Equations (13), Equation (20) does not affect the relevant Karush-Kuhn-Tucker (KKT) conditions described in the Appendix.

NRHO STATISTICAL MANEUVER ANALYSIS

Consider a preliminary statistical maneuver planning study along a selected L_2 Near Rectilinear Halo Orbit (NRHO). The true dynamics models for the spacecraft position $\boldsymbol{r}$ and velocity $\boldsymbol{v}$ are given in the rotating frame by

$$\begin{aligned}\dot{\boldsymbol{r}}(t) &= \boldsymbol{v}(t)\\ \dot{\boldsymbol{v}}(t) &= \nabla_r U + \boldsymbol{M}\boldsymbol{v}(t)\,,\end{aligned}$$

where

$$U = \frac{1-\mu}{\sqrt{(x+\mu)^2+y^2+z^2}} + \frac{\mu}{\sqrt{(x+\mu-1)^2+y^2+z^2}} + \frac{1}{2}(x^2+y^2)$$

$$\boldsymbol{M} = \begin{bmatrix} 0 & 2 & 0 \\ -2 & 0 & 0 \\ 0 & 0 & 0 \end{bmatrix}.$$

The components of the position vector, $\boldsymbol{r}$, are given by x, y, and z; $\boldsymbol{v}$ is the velocity vector as seen from the rotating frame, and $\mu = 0.01215058426$ is the mass ratio of the Earth-Moon system. All quantities are nondimensionalized by the conventional Earth-Moon values (DU $= 385,690$ km, TU $= 377,110$ seconds, and VU = DU/TU). Eight open loop impulsive maneuvers—four executed just before apolune and four just after—are optimized along with their associated feedback gains for dispersion control. These impulse times are fixed and are equally separated by three hours. The goal is to generate dispersion statistics (e.g., ΔV-99 intervals) for both the control and states from a single-shot optimization at points of interest along one revolution of the NRHO. These statistics are then compared to a Monte Carlo (MC) simulation that propagates samples from the given initial covariance $\boldsymbol{P}_{xx,0}$ using the optimized open loop impulses and feedback terms with numerical integration in between impulses.

The linearized, successive convexification (SCVX) approach is used for this application through CVX.[22] To build the discrete system for Equations (13), the continuous dynamics are linearized about the reference trajectory $\hat{\boldsymbol{x}}$ and discretized via numerical integration. Letting $\boldsymbol{f}^T = [\dot{\boldsymbol{r}}^T,\ \dot{\boldsymbol{v}}^T]$ and using the Jacobians of $\boldsymbol{f}$ evaluated at $\hat{\boldsymbol{x}}$, the state transition matrix (STM) for the ballistic dynamics are numerically integrated using Matlab's ODE45[23] between each discretization node. The relevant input data for the optimization is shown in Table 2—with the caveat that, though $N = 300$, there are only eight nodes where control is allowable. Since $\hat{\boldsymbol{x}}_0 = \boldsymbol{m}_{x,0} = \boldsymbol{m}_f$, it is expected that the magnitudes of optimized open loop controls be small since the mean trajectory should require minimal interference. Additionally, since the covariance values are much smaller than those for the mean in this application, the scaling method from Reference 13 is employed for solver stability.

Table 2. Optimization parameters for the NRHO maneuver planning scenario. Note that $\boldsymbol{m}_{x,0}$, $\hat{\boldsymbol{x}}_0$, and $\boldsymbol{m}_f$ are in nondimensional units.

Quantity	Value
$t_f - t_0$	1 revolution
N	300
$\boldsymbol{m}_{x,0} = \hat{\boldsymbol{x}}_0 = \boldsymbol{m}_f$	$[1.0213\ ,\ 0\ ,\ -0.1816\ ,\ 0\ ,\ -0.1018\ ,\ 0\ ]^T$
$\boldsymbol{P}_{xx,0} = \boldsymbol{P}_f$	$\begin{bmatrix} 30^2\boldsymbol{I}_3\ \text{km}^2 & \boldsymbol{0}_{3\times3} \\ \boldsymbol{0}_{3\times3} & 30^2\boldsymbol{I}_3\ (\text{cm/s})^2 \end{bmatrix}$
$\boldsymbol{F}_u$	$\begin{bmatrix} \boldsymbol{0}_{3\times3} \\ \boldsymbol{I}_3 \end{bmatrix}$
ρ_u	50 cm/s
γ	10

Optimization Results

The optimization performed three convex iterations for a total runtime of 20 seconds. The optimal mean trajectory and open loop impulse directions are illustrated in Figure 6 and similarly in Figure 7 for the y-z projection. Here, ER $= 6370$ km (i.e., Earth radii), and the covariance ellipses are scaled by a factor of eight for visibilty. The final optimized covariance remains within $\boldsymbol{P}_f$, as required. Figure 7 highlights the usual trend of covariance behavior for an NRHO starting from a spherical covariance at apolune; that is, the semimajor axis of the covariance starts to align with the orbit moving towards perilune, and once at perilune the covariance becomes long and "skinny."

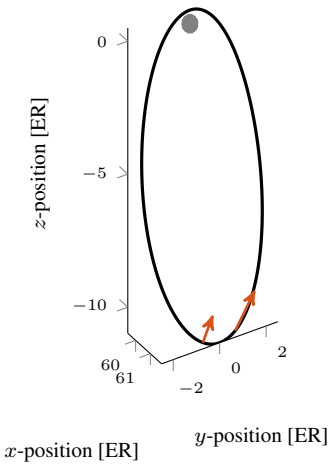

Figure 6. Reference NRHO and open loop impulse directions. Arrow scales represent relative impulse magnitudes.

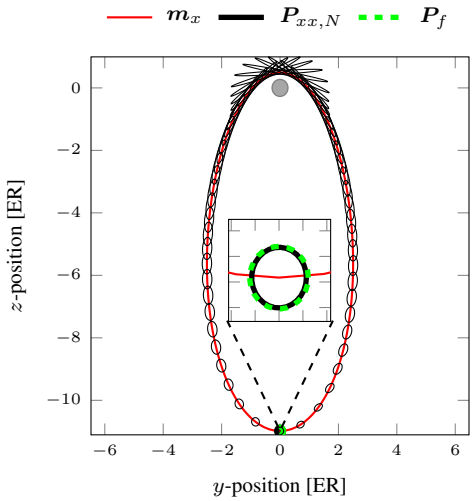

Figure 7. Optimal mean and covariance history. Covariances are scaled by a factor of eight.

Monte Carlo Results

Although the optimized terminal covariance remains within $\boldsymbol{P}_f$, as shown in Figure 7, this is within the linearized model used in the optimization. Thus, two MC simulation with 500 samples are conducted where, in the first MC, each sample is steered with natural dynamics only. In the

second MC, each sample is steered with closed-loop impulses via the optimized feedback gains and the continuous, natural dynamics. Figure 8 shows the terminal location of the samples, when subject to natural dynamics only, relative to $\boldsymbol{m}_f$, i.e., their error from $\boldsymbol{m}_f$, for the pair-wise combination of the six-dimensional state. Additionally, the terminal boundary covariances (i.e., $\boldsymbol{P}_f$) are depicted. A significant number of samples fall outside the prescribed boundary in all six dimensions. Thus, it can be said that, for the prescribed initial covariance $\boldsymbol{P}_{xx,0}$ in Table 2, a nonzero amount of dispersion control is required. Figure 9 shows the MC sample distributions at the terminal time when steered by the optimized feedback law. The MC sample distributions are well-characterized by the optimized covariances at the terminal time. Thus, in this scenario, the optimization successfully predicts the state dispersions. The dispersion of realized control magnitudes and the predicted 99% interval

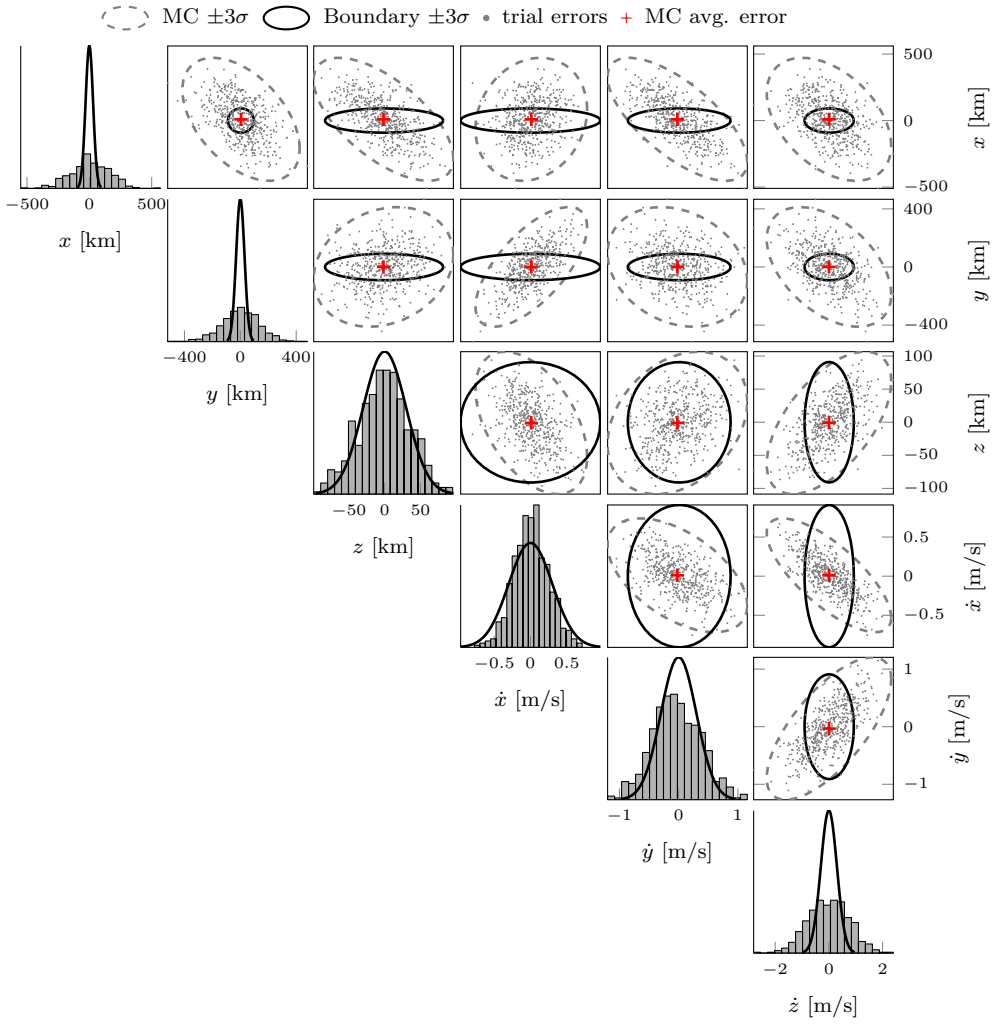

Figure 8. MC sample dispersions relative to the terminal mean state m_f with natural motion only.

from the optimization are shown via violin plots* in Figure 10. The realized control dispersions (i.e., closed-loop control samples) are shown for each control node, where the width of each cluster indicates the frequency at that magnitude. The optimization predicts the control dispersions without being overly conservative which is desired. Note the dispersions are skewed towards lower control

*For more information on violin plots, see Reference 24.

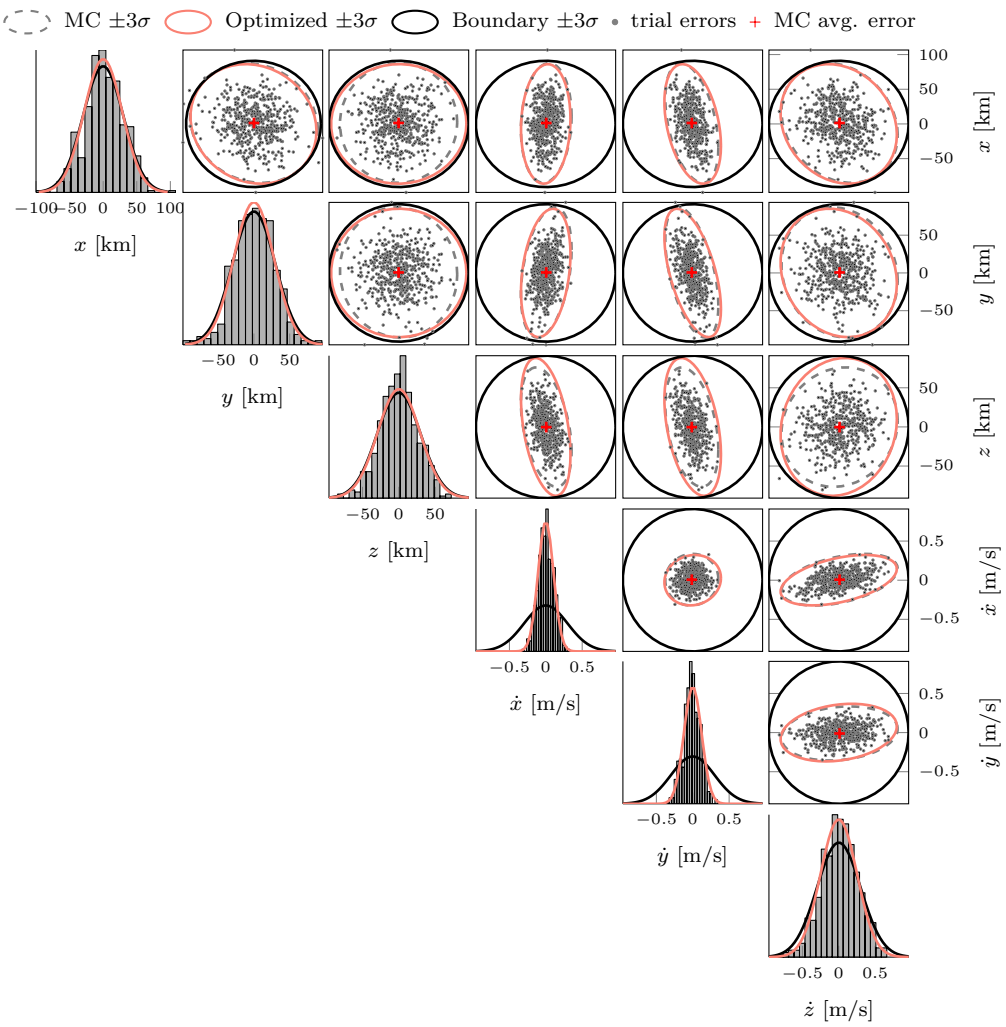

Figure 9. MC sample dispersions relative to the terminal mean state m_f along with the optimal and boundary covariances.

magnitudes, indicating that, on average, the state dispersions need only a small correction. Though

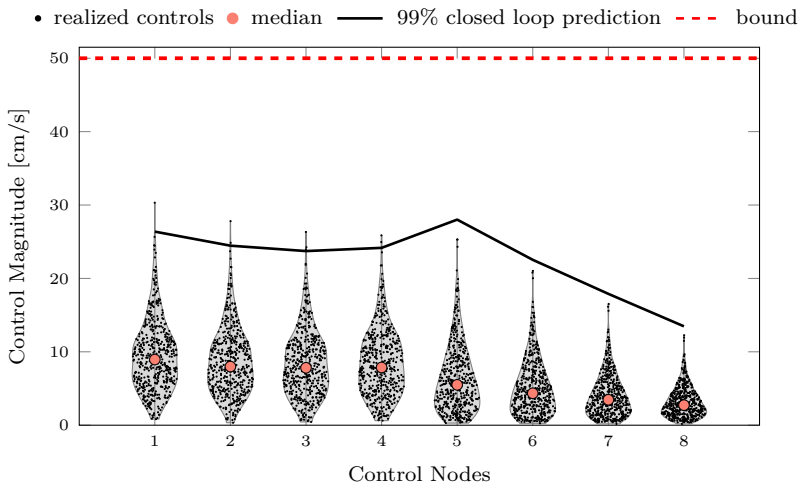

Figure 10. Control magnitude dispersions.

Figure 9 shows satisfactory results for the terminal dispersions, Figure 11 highlights the loss of covariance realism between the optimization and MC. Even with the amount of closed-loop control enacted before perilune (i.e., the first four nodes of Figure 10), the MC dispersions at perilune are heavily skewed and not well-characterized by the optimized covariance. Since the optimization has no size constraint on the perilune covariance, and since the combination of optimal closed loop controls and natural dynamics yields terminal constraint satisfaction, covariance realism is not guaranteed at perilune. This highlights the general possibility that covariance realism may be lost at times for which the optimization has no size constraint on the covariance.

Including Nonlinearity Constraints

To account for the loss of covariance realism in Figure 11, a second optimization is performed with the nonlinearity constraint from Equation (20). In this scenario, a probability gate $p = 0.99$ is used, and Equation (20) is split into constraints for position and velocity separately with $\beta_r = 500$ km and $\beta_v = 250$ m/s. These constraints are applied to the covariances at the first four impulse nodes. The unit-ball values for τ at these nodes for position and velocity are $\tau_r = [1746, 1600, 1474, 1367]$ and $\tau_v = [3.2, 2.9, 2.7, 2.5] \times 10^5$, respectively. Note that τ_v is much larger, indicating that linearization impacts the velocity state more than the position at perilune.

The optimization results for the nonlinearity constrained case are subjected to MC simulation as done before. The dispersion of realized control magnitudes is shown in Figure 12. As discussed, the nonlinearity constraint tends to increase the closed loop control usage due to the fact that a smaller covariance almost always decreases the measure of nonlinearity. This phenomena is clearly seen in Figure 12 for the control nodes before perilune (nodes 1-4). Figure 13 illustrates the MC dispersions at perilune, where it is now true that the optimized covariance well-captures the MC dispersions. Additionally, since perilune is the location for which nonlinearity is most significant, this constraint also results in covariance realism for all other time nodes. For comparison to the unconstrained case, the MC dispersions at the terminal time are also shown in Figure 14. Figures 9 and 14 show identical distributions for all state pairs except the $\dot{z}$ state, where it is clear the nonlinearity constrained case results in much smaller dispersions in that state at the terminal time. This is expected as a result of the $\dot{z}$ dispersions at perilune (in Figure 13) being nearly a third of

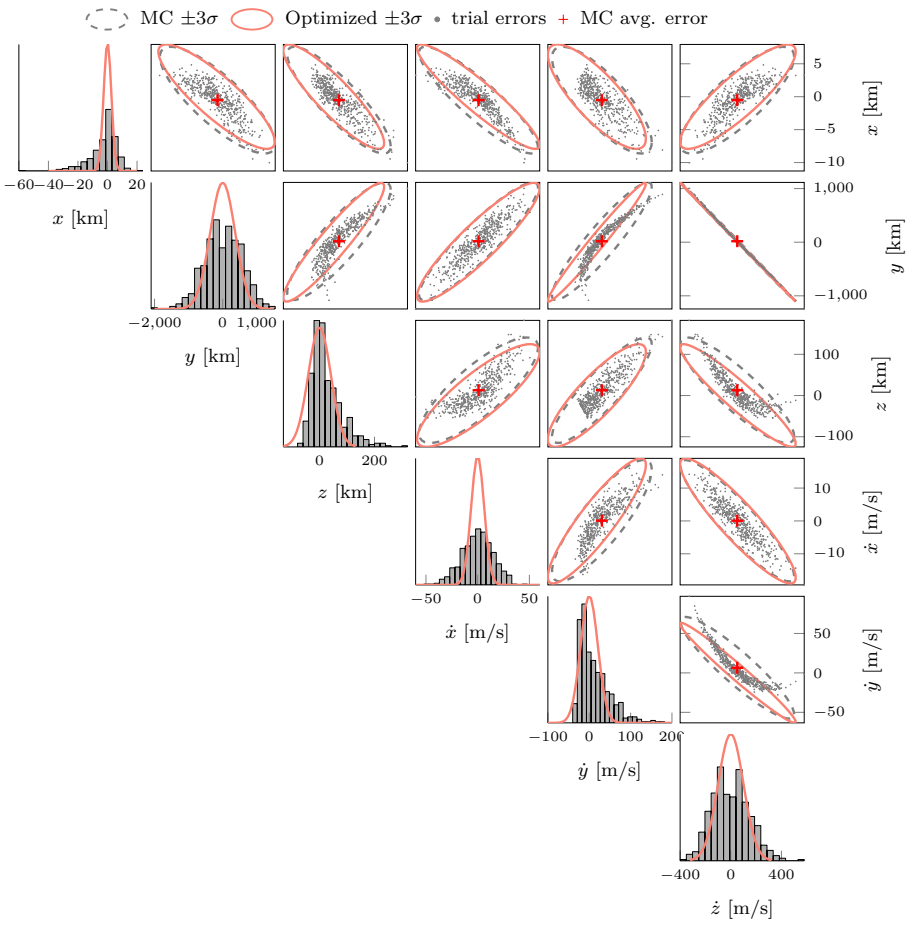

Figure 11. MC sample dispersions relative to the reference state $\hat{x}$ at perilune along with the optimal covariances.

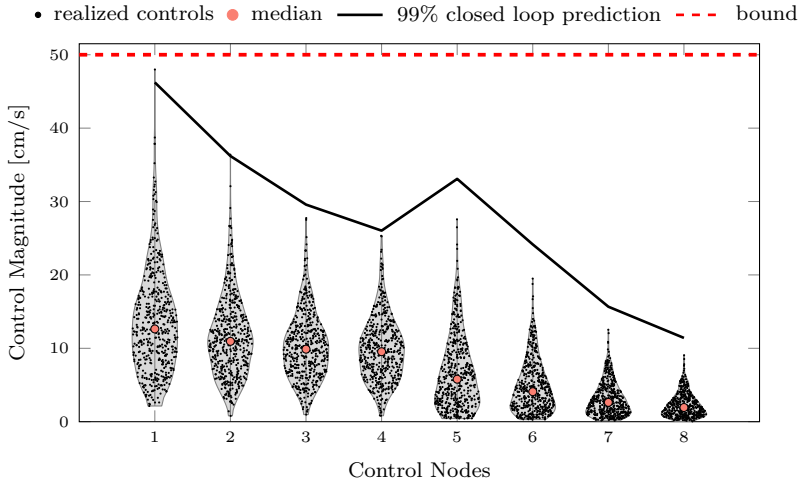

Figure 12. Control magnitude dispersions for the nonlinearity constrained case.

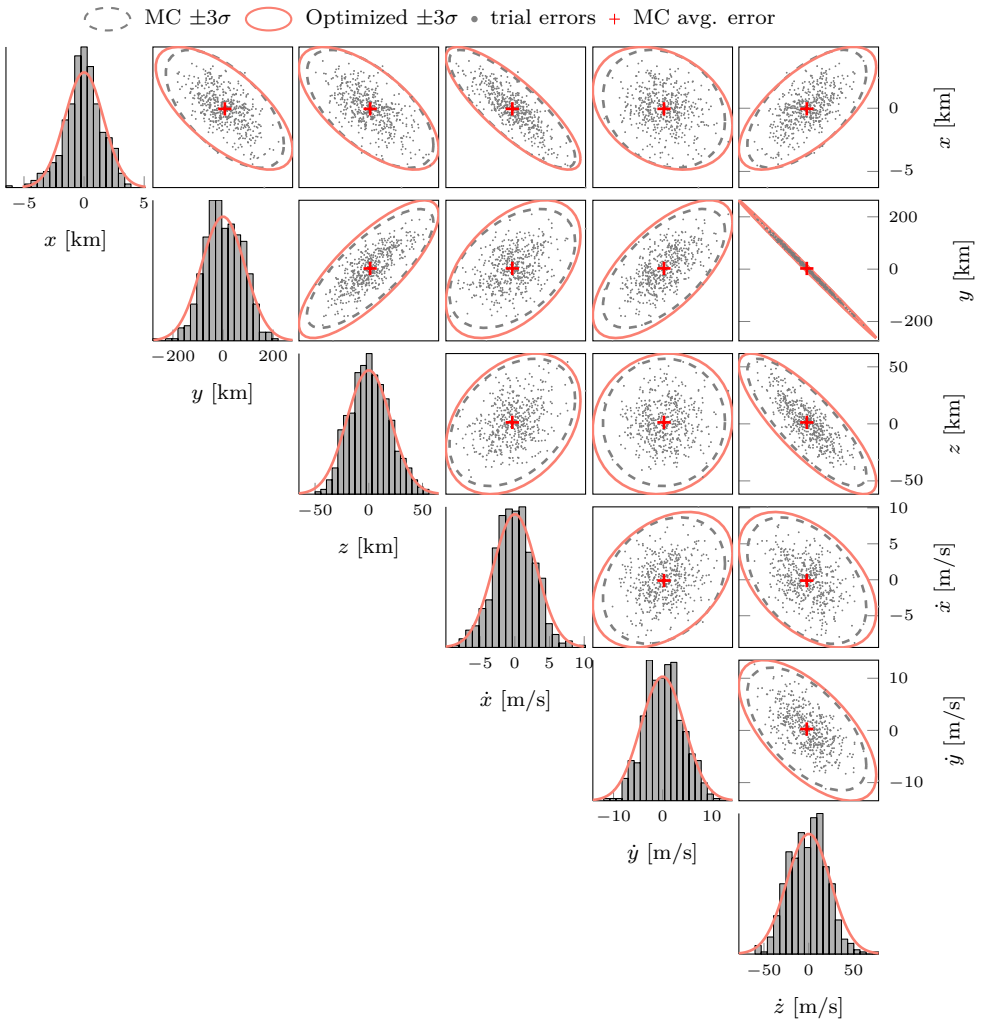

Figure 13. MC sample dispersions relative to the reference state $\hat{x}$ at perilune along with the optimal covariances for the nonlinearity constrained case.

their size from those in the unconstrained case (in Figure 11).

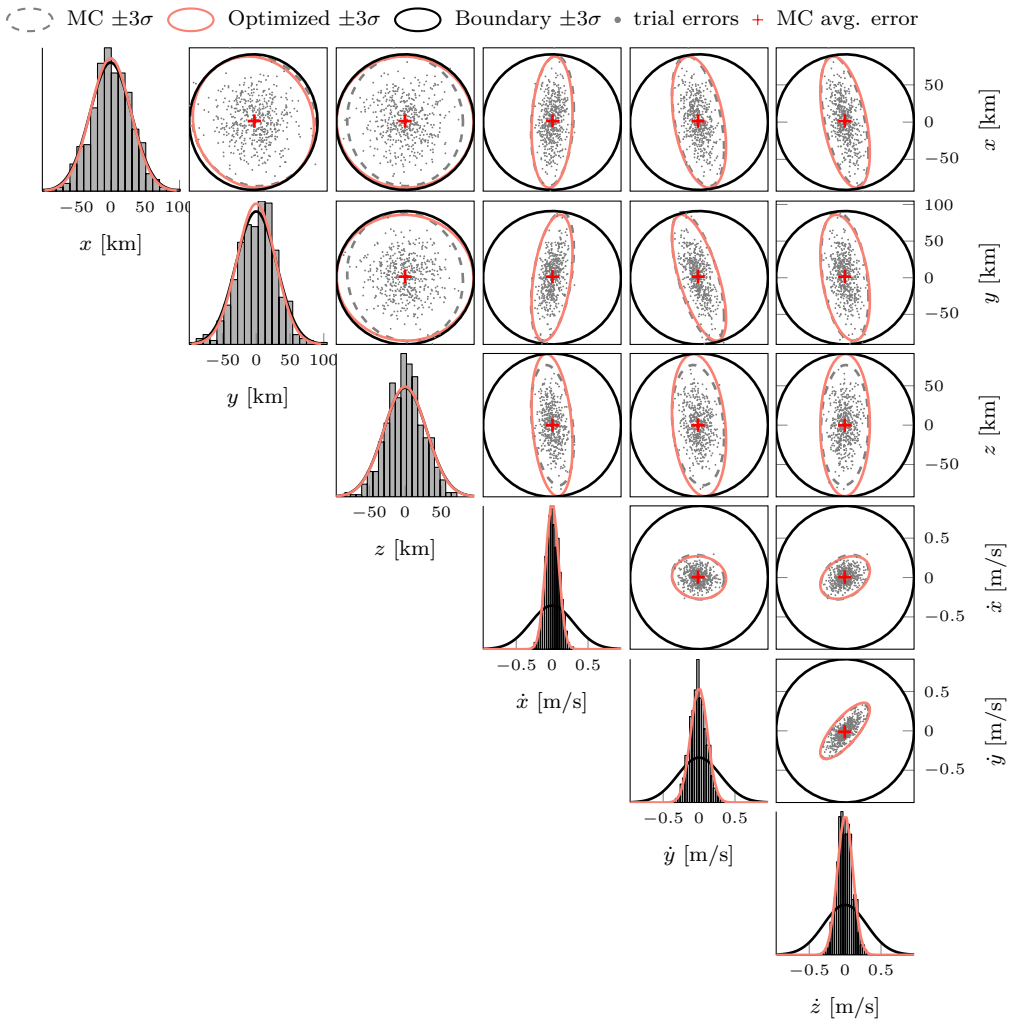

Figure 14. MC sample dispersions relative to the terminal mean state m_f along with the optimal and boundary covariances for the nonlinearity constrained case.

CONCLUSION

A key component of trajectory design is ensuring that the statistical dispersions of both the spacecraft state and control usage are minimized and/or constrained. In place of the common process involving repeating optimizations with deterministic state modeling assumptions, Gaussian steering has been proposed in the literature as a means of constructing—*a priori*—a feedback law to control state dispersions. This work introduces a general framework for a class of Gaussian steering problems to allow for multiple methods for mean and covariance approximation. Additionally, a nonlinearity constraint is introduced to ensure covariance realism such that the optimization well-captures the true dispersions.

The optimization framework is demonstrated on an L_2 Near Rectilinear Halo Orbit (NRHO) example wherein dispersions are kept within a prescribed covariance after one revolution of the

NRHO, as verified by Monte Carlo (MC) analysis. It is shown that, without the nonlinearity constraint, covariance realism is lost at perilune of the NRHO. Thus, a second optimization that includes a nonlinearity constraint is performed and a subsequent MC analysis establishes that covariance realism is satisfied at perilune. As expected, the increase in covariance realism in a highly nonlinear region of the state space requires larger amounts of closed-loop control. The NRHO application highlights the ability for Gaussian steering to extract dispersion statistics without MC analysis.

APPENDIX: LOSSLESS CONVEXIFICATION PROOF

From Equations (13), specifically Equation (13e), let

$$\boldsymbol{C}_k \triangleq \boldsymbol{U}_k \boldsymbol{P}_{xx,k}^{-1} \boldsymbol{U}_k^T - \boldsymbol{Y}_k \,, \tag{21}$$

such that requiring $\boldsymbol{C}_k$ to be negative semidefinite ($\boldsymbol{C}_k \preceq \boldsymbol{0}_{m\times m}$) is equivalent to Equation (13e) via the Schur complement.[25] Also let

$$\begin{aligned}
\boldsymbol{b}_k &= \hat{\boldsymbol{F}}_{x,k-1}\boldsymbol{m}_{x,k-1} + \boldsymbol{f}(\hat{\boldsymbol{x}}_{k-1}) - \hat{\boldsymbol{F}}_{x,k-1}\hat{\boldsymbol{x}}_{k-1} + \boldsymbol{F}_u\boldsymbol{v}_{k-1} - \boldsymbol{m}_{x,k} \\
\boldsymbol{H}_k &= \hat{\boldsymbol{F}}_{x,k-1}\boldsymbol{P}_{xx,k-1}\hat{\boldsymbol{F}}_{x,k-1}^T + \boldsymbol{F}_u\boldsymbol{U}_{k-1}\hat{\boldsymbol{F}}_{x,k-1}^T \\
&\quad + \hat{\boldsymbol{F}}_{x,k-1}\boldsymbol{U}_{k-1}^T\boldsymbol{F}_u^T + \boldsymbol{F}_u\boldsymbol{Y}_{k-1}\boldsymbol{F}_u^T + \boldsymbol{P}_{ww,k-1} - \boldsymbol{P}_{xx,k} \,,
\end{aligned}$$

such that $\boldsymbol{b}_k = \boldsymbol{0}_{n\times 1}$ and $\boldsymbol{H}_k = \boldsymbol{0}_{n\times n}$ are equivalent to Equations (13b) and (13c). The Lagrangian for Equations (13) is written as

$$L = \sum_{k=0}^{N-1} \text{tr}\{\boldsymbol{Y}_k\} + \boldsymbol{v}_k^T\boldsymbol{v}_k + \boldsymbol{\lambda}_k^T\boldsymbol{b}_k + \text{tr}\{\boldsymbol{\Lambda}_k^T\boldsymbol{H}_k\} + \phi_k(\|\boldsymbol{v}_k\| + \gamma\|\boldsymbol{Y}_k\|_F) + \text{tr}\{\boldsymbol{\Pi}_k^T\boldsymbol{C}_k\} \,, \tag{22}$$

where $\boldsymbol{\lambda}_k$, $\boldsymbol{\Lambda}_k$, ϕ_k, and $\boldsymbol{\Pi}_k$ are Lagrange multipliers and $\boldsymbol{\Lambda}_k$ and $\boldsymbol{\Pi}_k$ are symmetric. It has been shown in Reference 7 that, for a deterministically controllable system, Equations (13) satisfy Slater's conditions for strict feasibility, and since the problem is convex, this means strong duality holds, and the KKT conditions for Equation (22) are sufficient conditions for an optimum. This proof leverages a contradiction in the KKT conditions for Equation (22) when $\boldsymbol{C}_k \neq \boldsymbol{0}_{m\times m}\ \forall k$. The relevant KKT conditions are[7]

$$\frac{\partial L}{\partial \boldsymbol{U}_k} = \boldsymbol{\Pi}_k\boldsymbol{U}_k\boldsymbol{P}_{xx,k}^{-1} + \boldsymbol{F}_u^T\boldsymbol{\Lambda}_k\hat{\boldsymbol{F}}_{x,k-1} = \boldsymbol{0}_{m\times n} \tag{23a}$$

$$\frac{\partial L}{\partial \boldsymbol{Y}_k} = \boldsymbol{I}_m - \boldsymbol{\Pi}_k + \boldsymbol{F}_u^T\boldsymbol{\Lambda}_k\boldsymbol{F}_u + \phi_k\gamma\frac{\boldsymbol{Y}_k}{\|\boldsymbol{Y}_k\|_F} = \boldsymbol{0}_{m\times m} \tag{23b}$$

$$\text{tr}\{\boldsymbol{\Pi}_k^T\boldsymbol{C}_k\} = 0 \tag{23c}$$

$$\boldsymbol{C}_k \preceq \boldsymbol{0}_{m\times m} \,, \quad \boldsymbol{\Pi}_k \succeq \boldsymbol{0}_{m\times m} \,, \quad \boldsymbol{Y}_k \succeq \boldsymbol{0}_{m\times m} \,, \quad \boldsymbol{P}_{xx,k} \succeq \boldsymbol{0}_{n\times n} \,, \quad \phi_k \geq 0 \,, \tag{23d}$$

where Equation (23c) is the complementary slackness condition and Equation (23d) is true by problem construction. Using Lemma 1 of Reference 7, the Lagrange multiplier $\boldsymbol{\Pi}_k$ must be singular if $\boldsymbol{C}_k$ has at least one nonzero eigenvalue due to Equation (23c). If $\boldsymbol{\Pi}_k$ is nonsingular, $\boldsymbol{C}_k = \boldsymbol{0}_{m\times m}$. Substituting $\boldsymbol{F}_u^T\boldsymbol{\Lambda}_k$ from Equation (23a) into Equation (23b) results in

$$\boldsymbol{I}_m + \phi_k\gamma\frac{\boldsymbol{Y}_k}{\|\boldsymbol{Y}_k\|_F} = \boldsymbol{\Pi}_k(\boldsymbol{I}_m + \boldsymbol{U}_k\boldsymbol{P}_{xx,k}^{-1}\hat{\boldsymbol{F}}_{x,k-1}^{-1}\boldsymbol{F}_u) \,. \tag{24}$$

Note that it is assumed that $\hat{\boldsymbol{F}}_{x,k-1}$ is invertible $\forall\ k$. Taking the determinant of both sides gives

$$\det\left(\boldsymbol{I}_m + \phi_k\gamma\frac{\boldsymbol{Y}_k}{\|\boldsymbol{Y}_k\|_F}\right) = \det(\boldsymbol{\Pi}_k)\det(\boldsymbol{I}_m + \boldsymbol{U}_k\boldsymbol{P}_{xx,k}^{-1}\hat{\boldsymbol{F}}_{x,k-1}^{-1}\boldsymbol{F}_u)\,. \tag{25}$$

By construction, $\boldsymbol{Y}_k \succeq \boldsymbol{0}_{m\times m}$, and, therefore, the left-hand side of Equation (25) is always positive; thus, $\boldsymbol{\Pi}_k$ must be nonsingular and $\boldsymbol{C}_k = \boldsymbol{0}_{m\times m}$ for all k at the optimum.

REFERENCES

[1] A. E. Bryson and Y.-C. Ho, *Applied Optimal Control: Optimization, Estimation and Control*. Wiley, 1975.

[2] L. Blackmore, "Autonomous Precision Landing of Space Rockets," *Frontiers of Engineering: Reports on Leading-Edge Engineering from the 2016 Symposium*, Vol. 46, The Bridge Washington, DC, pp. 15–20.

[3] K. Okamoto, M. Goldshtein, and P. Tsiotras, "Optimal Covariance Control for Stochastic Systems Under Chance Constraints," *IEEE Control Systems Letters*, Vol. 2, No. 2, 2018, pp. 266–271.

[4] I. M. Ross, R. J. Proulx, and M. Karpenko, "Unscented Trajectory Optimization," *Journal of Guidance, Control, and Dynamics*, Vol. 48, No. 1, 2025, pp. 20–31, 10.2514/1.G007925.

[5] E. Bakolas, "Optimal Covariance Control for Discrete-Time Stochastic Linear Systems Subject to Constraints," *55th IEEE Conference on Decision and Control (CDC)*, 2016, pp. 1153–1158, 10.1109/CDC.2016.7798422.

[6] I. M. Balci and E. Bakolas, "Covariance Steering of Discrete-Time Stochastic Linear Systems Based on Distribution Distance Terminal Costs," *arXiv preprint arXiv:2009.14252*, 2020.

[7] F. Liu, G. Rapakoulias, and P. Tsiotras, "Optimal Covariance Steering for Discrete-Time Linear Stochastic Systems," *IEEE Transactions on Automatic Control*, Vol. 70, No. 4, 2025, pp. 2289–2304, 10.1109/TAC.2024.3472788.

[8] J. Ridderhof, J. Pilipovsky, and P. Tsiotras, "Chance-Constrained Covariance Control for Low-Thrust Minimum-Fuel Trajectory Optimization," *AAS/AIAA Astrodynamics Specialist Conference*, No. 20-618, 2020.

[9] W. Fife, P. Ghosh, and K. J. DeMars, "Probabilistic Trajectory Design Via Approximate Gaussian Mixture Steering," *AAS/AIAA Astrodynamics Specialist Conference*, 2024.

[10] K. Oguri, "Chance-Constrained Control for Safe Spacecraft Autonomy: Convex Programming Approach," *2024 American Control Conference (ACC)*, IEEE, 2024, pp. 2318–2324.

[11] E. L. Jenson and D. J. Scheeres, "Semianalytical Measures of Nonlinearity Based on Tensor Eigenpairs," *Journal of Guidance, Control, and Dynamics*, Vol. 46, No. 4, 2023, pp. 638–653, 10.2514/1.G006760.

[12] J. Kulik, C. Orton-Urbina, M. Ruth, and D. Savransky, "Applications of Induced Tensor Norms to Guidance Navigation and Control," *arXiv preprint arXiv:2408.15362*, 2024.

[13] N. Kumagai and K. Oguri, "Sequential Chance-Constrained Covariance Steering for Robust Cislunar Trajectory Design under Uncertainties," *AAS/AIAA Astrodynamics Specialist Conference*, No. 24-379, 2024.

[14] K. Oguri and G. Lantoine, "Stochastic Sequential Convex Programming for Robust Low-Thrust Trajectory Design Under Uncertainty," *AAS/AIAA Astrodynamics Specialist Conference*, No. 22-708, 2022.

[15] J. T. Betts, *Practical Methods for Optimal Control Using Nonlinear Programming*. SIAM, 2010.

[16] G. Rapakoulias and P. Tsiotras, "Discrete-Time Optimal Covariance Steering via Semidefinite Programming," *2023 62nd IEEE Conference on Decision and Control (CDC)*, IEEE, 2023, pp. 1802–1807.

[17] D. Malyuta, T. P. Reynolds, M. Szmuk, T. Lew, R. Bonalli, M. Pavone, and B. Açıkmeşe, "Convex Optimization for Trajectory Generation: A Tutorial on Generating Dynamically Feasible Trajectories Reliably and Efficiently," *IEEE Control Systems Magazine*, Vol. 42, No. 5, 2022, pp. 40–113, 10.1109/MCS.2022.3187542.

[18] K. Oguri, "Successive Convexification with Feasibility Guarantee via Augmented Lagrangian for Non-Convex Optimal Control Problems," *62nd IEEE Conference on Decision and Control (CDC)*, 2023, pp. 3296–3302, 10.1109/CDC49753.2023.10383462.

[19] I. Arasaratnam, S. Haykin, and R. J. Elliott, "Discrete-Time Nonlinear Filtering Algorithms Using Gauss–Hermite Quadrature," *Proceedings of the IEEE*, Vol. 95, No. 5, 2007, pp. 953–977, 10.1109/JPROC.2007.894705.

[20] S. Julier and J. Uhlmann, "Unscented Filtering and Nonlinear Estimation," *Proceedings of the IEEE*, Vol. 92, No. 3, 2004, pp. 401–422, 10.1109/JPROC.2003.823141.

[21] P. E. Gill, W. Murray, and M. A. Saunders, "SNOPT: An SQP Algorithm for Large-Scale Constrained Optimization," *SIAM Review*, Vol. 47, No. 1, 2005, pp. 99–131.

[22] M. GRANT, "CVX: Matlab Software for Disciplined Convex Programming, Version 1.21," *http://cvxr. com/cvx, Apr.*, 2011.

[23] L. F. Shampine and M. W. Reichelt, "The Matlab ODE Suite," *SIAM Journal On Scientific Computing*, Vol. 18, No. 1, 1997, pp. 1–22.

[24] J. L. Hintze and R. D. Nelson, "Violin Plots: A Box Plot-Density Trace Synergism," *The American Statistician*, Vol. 52, No. 2, 1998, pp. 181–184, 10.1080/00031305.1998.10480559.

[25] G. H. Golub and C. F. Van Loan, *Matrix Computations*. JHU press, 2013.